Detection of Magnetic Fields Highly Attenuated by the Skin Effect Through a Ferrous Steel Boundary Using a Super Narrow-Band Digital Filter

Patrick Gaydecki, *Senior Member, IEEE*, Graham Miller, Muhammad Zaid, Bosco Fernandes, and Haitham Hussin

***Abstract*—A complete instrumentation system is described that is capable of launching alternating magnetic fields through a large mild steel plate that is 2 mm in thickness and detecting them on the face opposite from the transmitter with remarkable signal-to-noise ratios. Results for signal frequencies ranging between 4.5 and 13 kHz are reported. The skin depth at 9 kHz for the steel used is approximately 137 μm. The detection of the minute fields arriving at the receiving coil is made possible by the use of digitally synthesized input signals, low-noise amplification, and, in particular, the use of a powerful real-time digital signal processing system that isolates the signal of interest using a super narrow-band filter and very high levels of distortion-free gain. Although traditional methods of weak signal detection, such as lock-in amplification, may also be applied in this context, the digital approach discussed here is both more cost effective and flexible, allowing the simultaneous detection of multiple frequencies.**

***Index Terms*—Digital narrow-band filter, lock-in amplification, skin effect, weak field detection.**

I. Introduction

THERE ARE numerous occasions when it is desirable to transmit a time-varying magnetic field through a metal structure and detect the signal that has traveled through the material, either in a reflectance mode or in a through-transmission mode. Examples include nondestructive testing, remote field eddy current (RFEC) inspection, materials characterization, and security screening [1]–[5]. A time-varying magnetic field will induce eddy currents in a target, such as a steel plate, which, in turn, generate magnetic fields throughout the plate thickness.

Due to the skin effect, however, which is defined as the tendency of a high-frequency electric current to distribute itself inside a conductor so that the current density is greatest at the surface, the strength of both the eddy currents and the associated magnetic field fall rapidly with depth in ferrous materials. The equation that describes the fall in the current density is given by

$$J = J_s e^{-\frac{d}{\delta}} \cdot e^{j\left(\omega t - \frac{d}{\delta}\right)} \tag{1}$$

where J_s is the current density on the surface, d is the depth within the material, δ is the skin depth, ω is the angular frequency, and J is the current density at depth d. The skin depth for a given material is governed by the relationship

$$\delta = \sqrt{\frac{2}{\omega \mu_0 \mu_r \sigma}} \tag{2}$$

where σ is the conductivity of the conductor or target, μ_r is its relative permeability, and μ_0 is the absolute permeability of a vacuum. The skin effect severely constrains the operational frequency range of eddy current equipment, which is a factor that limits its ability to detect and resolve small features at depth. In this paper, however, we describe an instrumentation system that is capable of launching alternating magnetic fields through a mild steel plate that is 2 mm in thickness and detecting them on the face opposite from the transmitter with exceptional purity. Because material properties vary in practice, it is difficult to know the precise values of the conductivity and permeability of a mild steel sample and, thus, obtain an accurate measure of its skin depth. Moreover, the permeability of magnetic materials is not constant, and it changes over a several-decade range as the excitation level is varied. Often, the permeability value given in tables is the maximum permeability or the maximum relative permeability for a specific material. The maximum permeability is the point where the slope of the B/H curve for the unmagnetized material is the greatest. This is often taken as the point where a straight line from the origin is tangential to the B/H curve. Here, the permeability has been chosen to be of a low value because, at the small applied field strengths, it is an incremental permeability associated with a minor hysteresis loop, rather than the typically tabulated maximum permeability of a full B/H loop.

Assuming, therefore, conservative figures for the conductivity as 6.0×10^6 S $\cdot$ m^{-1} and a relative permeability of 250, a skin depth of 0.194 mm is obtained at 4.5 kHz and 0.137 mm at 9 kHz. From (1), it is clear that for an excitation frequency of 4.5 kHz, the (eddy) current density at a depth of 2 mm is approximately equal to 0.33×10^{-4} of its value at the surface. Since the magnetic field is proportional to the current, the field

Manuscript received December 8, 2005; revised November 22, 2007. This work was supported by the Great Man-Made River Authority, Libya.

P. Gaydecki and B. Fernandes are with the School of Electrical and Electronic Engineering, The University of Manchester, Manchester M60 1QD, U.K. (e-mail: patrick.gaydecki@manchester.ac.uk).

G. Miller is with the Space Research Centre, University of Leicester, Leicester LE1 7RH, U.K.

M. Zaid is with the School of Applied Sciences, The University of Northampton, Northampton NN2 7AL, U.K.

H. Hussin is with the Great Man-Made River Authority, Benghazi, Libya.

Color versions of one or more of the figures in this paper are available online at http://ieeexplore.ieee.org.

Digital Object Identifier 10.1109/TIM.2007.915150

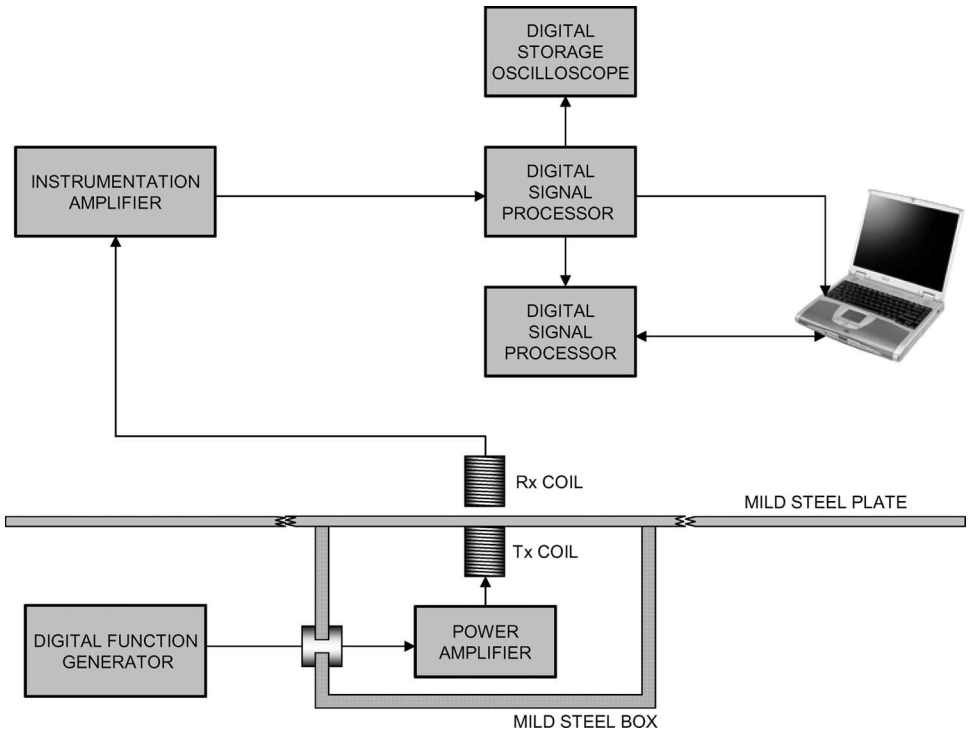

Fig. 1. Instrumentation configuration.

radiated on the back face of the plate will experience similar levels of attenuation. For an excitation frequency of 9 kHz, the attenuation at a depth of 2 mm is approximately 0.457×10^{-6}.

The success of the detection systems is predicated on the design and use of digitally synthesized stable excitation signals, low-noise instrumentation amplifiers, a powerful real-time digital signal processing (DSP) system that performs super narrow-band filtering, and a very high resolution analog-to-digital and digital-to analog (codec) converter.

II. Instrumentation and Experimental Configuration

A. System Hardware

Fig. 1 depicts the instrumentation used to transmit and detect the high-frequency magnetic fields. A 50-mV peak-to-peak sinusoidal signal at a single frequency was synthesized by a Thurlby Thandar TGA1230 digital function generator. This was fed to a current power amplifier, with a voltage gain of 30 dB, whose output was, in turn, connected to the transmitter coil. The coil, which was commercially obtained, was wound from a 0.2-diameter copper wire; the coil itself had an external diameter of 15.2 mm, was 10 mm in length, and was wound around a ferrite core with a diameter of 13 mm. The ferrite core was topped with a 3-mm flange made of the same material, with an external diameter of 16 mm. The inductance at 10 kHz was 4.7 mH, as measured by an HP 4192A impedance analyzer. The currents flowing through the coil at 4.5 and 9 kHz were measured to be 7.5 and 3.8 mA, respectively.

Three methods were used to obtain and cross-check the magnetic flux density of the energized coil at its end surface: 1) by direct measurement using a Hirst GM04 Gauss meter

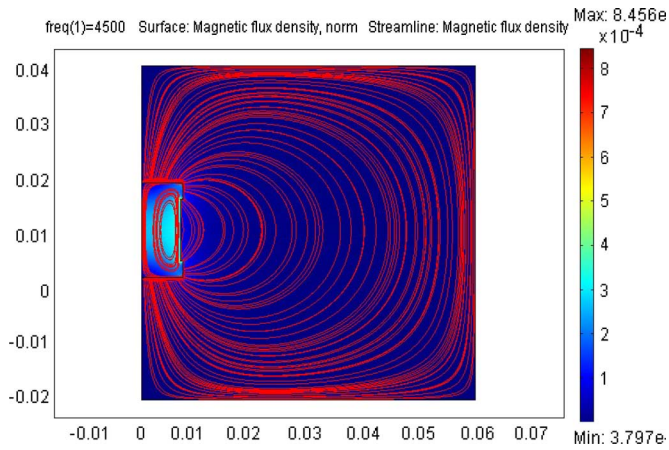

Fig. 2. Finite-element image of the transmitter coil produced by the modeling package *Femlab*, with which the magnetic field density at the top surface of the coil was estimated.

(Hirst Magnetic Instruments Ltd.); 2) by directly using the Biot–Savart law; and 3) by using the finite-element modeling package *Femlab* (Fig. 2). Using these methods, the magnetic flux densities at 9 kHz were estimated to be 0.031, 0.021, and 0.03 mT, respectively. These values were broadly consistent with one another and in general agreement with measured field strengths attenuated by the plate (see Section III-A). As indicated in Fig. 1, the coil was enclosed within a rectangular-section mild steel box with a wall thickness of 1 mm. The box was 100 mm in height, 200 mm in width, and 200 mm in length. In place of a lid, a steel plate was placed over the box, and the transmitter coil was mounted at its center. The steel plate was 2 mm in thickness and 1000 $\times$ 1300 mm in area. The dimensions of the plate were selected to be much larger than those of the transmitter coil to minimize edge effects,

which dominate at higher frequencies, and to reduce coupling of the excitation and sensing coils around the edges of the plate. The receiver coil was of identical dimensions to the transmitter but had an inductance of 11 mH. It was attached to a scanner arm on the opposite face of the plate at a height of either 3 or 10 mm and aligned such that when scanned across its shorter dimension, it crossed the location of the transmitter coil. The receiver coil outputs were applied to a low-noise wide-band instrumentation amplifier (10 Hz to 4 MHz), which was designed with a moderate gain of 400 (52 dB). The signal produced by the amplifier was then fed to a real-time DSP system.

The DSP system comprised a high-level Windows-based user interface that designed the filters and a hardware module that executed the filters in real time. The main processing element of the DSP system was a DSP56309 (Freescale Semiconductor, Inc.), operating at 100 million multiplication-accumulations/s. This processor is a single clock-cycle per instruction cycle machine, incorporating a 24-bit, fixed-point, fractional arithmetic logic unit (ALU), super Harvard architecture with 20 kB of code memory space and 14 kB of data memory space [6]. To take advantage of the large dynamic range of the ALU (144 dB), the processor was interfaced to a Cirrus CS4271 dual-channel 24-bit sigma–delta codec sampling at 48 kHz. The DSP system was employed both to perform super narrow-band filtering and to apply high levels of digital gain with exceptional purity. The output of the DSP system was fed both to a digital oscilloscope for signal capture and to a second identical DSP system, which performed a real-time spectral analysis of the signals.

B. Design of the Filter and Digital Gain Stage

As confirmed by the skin-depth calculations, the raw signal detected by the receiving coil was extremely weak; it was also embedded in background noise (both electronic and environmental in origin), which typically has a $1/f$ distribution. Amplification alone would not extract the signal, and therefore, filtering was required. However, filtering will only be successful if a sufficient noise bandwidth can be suppressed while leaving the signal bandwidth unaffected. The weaker the signal, the more specific the filter must be. Because of the extreme nature of the problem, an analog approach would have been unacceptable, since it is virtually impossible using this methodology to design and implement filters with the required frequency precision, transition zone performance, and stability. Digital filters are typically realized using either a finite impulse response (FIR) or an infinite impulse response (IIR) approach. In the former case, the convolution expression is given by

$$y[n] = \sum_{k=0}^{M-1} h[k]x[n-k] \tag{3}$$

where $x[n]$, $y[n]$, and $h[n]$ are the input signal, output signal, and convolution kernel (impulse response), respectively. According to the duality principle of the Fourier transform, the narrower the filter is in the frequency domain, the longer its impulse response must be in the time domain. In this application, a bandwidth of 2 Hz within a frequency range of 24 kHz was demanded. Such selectivity would require the kernel of the FIR filter to comprise approximately 30 000 coefficients, effectively ruling out real-time operation. In contrast, IIR filters rely on recurrence formulas, where the output signal is given by

$$y[n] = \sum_{k=0}^{N} a[k]x[n-k] - \sum_{k=1}^{M} b[k]y[n-k]. \tag{4}$$

Because of their recursive nature, IIR filters impose less computational burden on the processor than FIR types, requiring fewer coefficients to achieve the same cutoff performance. In fact, it is possible to design a low-order narrow-band filter with as narrow a bandwidth as desired by placing the poles of the filter sufficiently close to the unit circle in the z-plane. In this case, a super narrow-band IIR filter was designed in software using the pole–zero placement method [6]. Given a second-order filter expressed in factored form, the transfer function becomes

$$H(z) = \prod_{k=0}^{n-1} \frac{z - z_k}{z - p_k} \tag{5}$$

where z_k and p_k represent the zeros and poles of the filter, respectively. Since the zeros and poles are conjugates, their complex values are

$$\begin{aligned} z_0 &= \alpha_0 + j\beta_0 \\ z_1 &= \alpha_0 - j\beta_0 \\ p_0 &= \alpha_1 + j\beta_1 \\ p_1 &= \alpha_1 - j\beta_1. \end{aligned} \tag{6}$$

Simplifying

$$\begin{aligned} d_0 &= \alpha_0^2 + \beta_0^2 \\ d_1 &= \alpha_1^2 + \beta_1^2. \end{aligned} \tag{7}$$

Then, each second-order stage is given by

$$\begin{aligned} H(z) &= \frac{[z - (\alpha_0 + j\beta_0)]\,[z - (\alpha_0 - j\beta_0)]}{[z - (\alpha_1 + j\beta_1)]\,[z - (\alpha_1 - j\beta_1)]} \\ &= \frac{1 - 2\alpha_0 z^{-1} + \varepsilon_0 z^{-2}}{1 - 2\alpha z^{-1} 1 + \varepsilon_1 z^{-2}}. \end{aligned} \tag{8}$$

The difference equation for each second-order stage is therefore

$$\begin{aligned} y[n] = x[n] - 2\alpha_0 x[n-1] + \varepsilon_0 x[n-2] \\ + 2\alpha_1 y[n-1] - \varepsilon_1 y[n-2]. \end{aligned} \tag{9}$$

The high-level software takes as its inputs the pole and zero locations for the filter, calculates the IIR coefficients, and downloads them to the DSP hardware module, which then implements (4) in real time. Two such narrow-band filters were designed for 4.5 and 9 kHz. Table I gives the locations of the poles; all zeros had the value zero.

The resonance point of a narrow-band digital filter is determined by the position of the poles on the unit circle, which is

TABLE I
POLE LOCATIONS FOR THE TWO IIR FILTERS

Centre Frequency, kHz	p_0, real	p_0, imaginary	p_1, real	p_1, imaginary
4.5	0.83146	0.55556	0.83146	-0.55556
9.0	0.38268	0.92387	0.38268	-0.92387

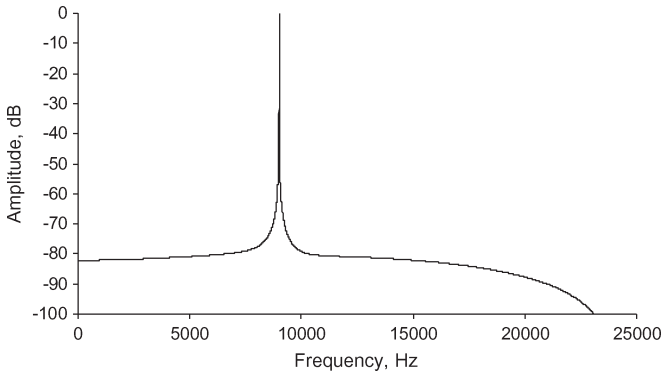

Fig. 3. Frequency response of the super narrow-band filter at 9 kHz. Note the decibel scale of the amplitude axis.

given by the Cartesian coordinates and specified as a complex number. The angle that a pole subtends to the origin is equal to ωT (T being the sample period), and this determines the frequency. Furthermore, the closer the pole is located to the circumference of the unit circle, the higher the Q-factor. In our case, the poles are very close to the circumference, resulting in a filter with an extreme selectivity. Fig. 3 depicts the frequency response of the filter with a center frequency of 9 kHz.

Although it is not possible to discern this from Fig. 3, the filter has a bandwidth of less than 2 Hz (-3-dB points) and is located precisely at the desired frequency. Since it has a very narrow bandwidth, its impulse response decay time lasts for approximately 5 s. The filter at 4.5 kHz had similar properties. After filtering, the signal was digitally postamplified by a factor of 4096 and fed to the digital-to-analog section of the codec, and from there, it was sent as a voltage to the oscilloscope. In total, the gain applied to the (filtered) signal was 1 638 400 (or 124 dB).

III. RESULTS

Using a motorized laboratory scanner, the receiver coil was tracked across the surface of the plate, and at 20-mm intervals, the root-mean-square (rms) voltage of the processed and amplified signal was measured by the digital oscilloscope. Fig. 4(a) depicts the results obtained from a scan in which an excitation frequency of 4.5 kHz was used, with the receiver located 10 mm above the steel surface. This distance was chosen for issues relating to the ease of scanning; however, a future objective of the study will be to detect fields at much greater standoff distances since the plates will, in practice, be embedded within concrete. The central peak in Fig. 4(a) corresponds to the exact position of the transmitter coil. The tails at the left and right extremes of the plot are due to edge effect leakage. Fig. 4(b) is a spectrum of the signal obtained when the receiver coil was directly above the transmitter; this spectrum was obtained

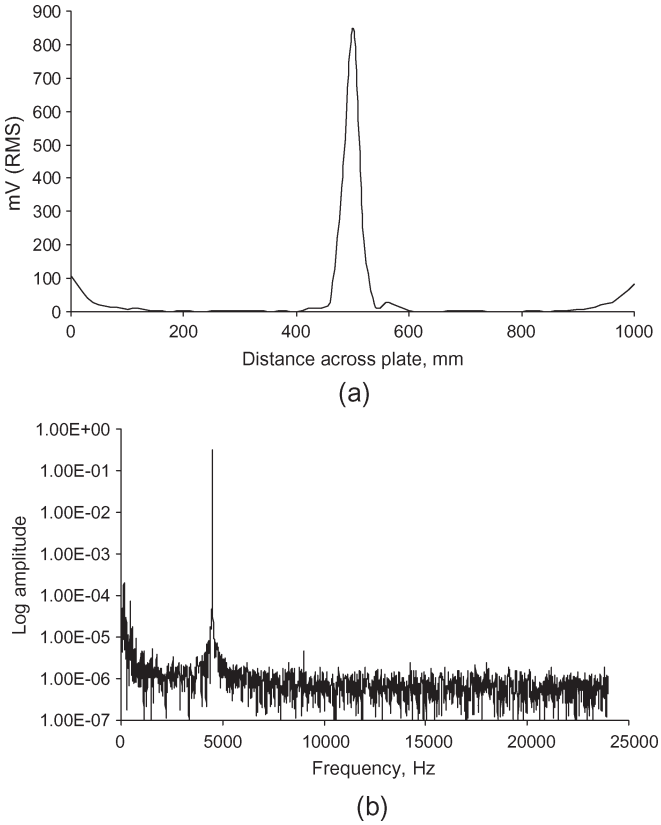

Fig. 4. (a) Line scan result at 4.5 kHz and a liftoff of 10 mm. (b) Fourier spectrum of the processed signal with the receiver coil located above the transmitter.

using the second signal processor, which, as stated, employs 24-bit resolution. Fig. 5(a) and (b) shows the data obtained using an excitation frequency of 9 kHz and a scan height of 3 mm. Although the edge effects are much stronger and the signal peak is weaker, there is no question that the system is indeed detecting the signal propagated through the steel barrier.

To establish the detection limit of the instrumentation, the excitation frequency of the signal applied to the transmitter was increased, and the digital filter was accordingly redesigned; reconfiguring the DSP system requires only a few seconds. Specifically, measurements were taken at frequencies of 12 and 13 kHz, and in both cases, the signal was unambiguously recovered from the noise.

A. Instrument Calibration and Quantitative Measurements

To calibrate the system and, hence, convert the signal magnitudes returned by the instrument into magnetic flux densities, the receiver coil was exposed to an ac magnetic field at several spot frequencies with a known magnetic flux density of 1 μT, as measured by an *EMFields Professional ELF Magnetic Field Meter* (Perspective Scientific Ltd.), which has a measurement range of 0–20 μT and a resolution of 10^{-8} T. By this means, it was determined that the flux densities for the fields propagated through the plate at 9, 11, and 13 kHz were 7.89×10^{-11}, 1.89×10^{-11}, and 8.99×10^{-12} T, respectively.

It was previously calculated that at 9 kHz, the skin effect would result in an attenuation of 0.457×10^{-6}, with an

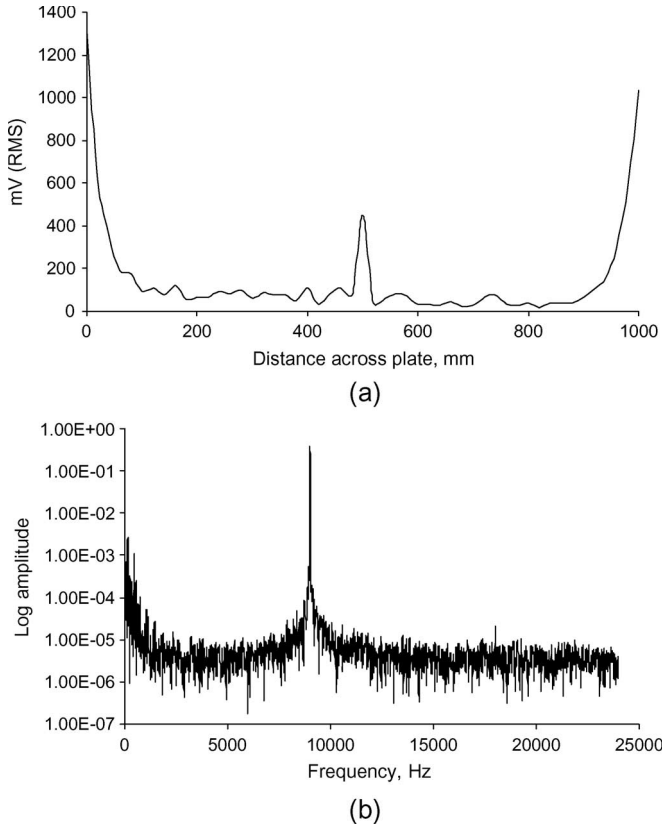

Fig. 5. (a) Line scan result at 9 kHz and a liftoff of 3 mm. (b) Fourier spectrum of the processed signal with the receiver coil located above the transmitter.

estimated field strength on the top surface of the transmitter coil of approximately 0.03 mT (Section II); by this estimate, the flux density on the far side of the plate would be 1.371×10^{-11} T, which is within a factor of 5.8 of the measured value. Given that predicting flux densities is notoriously difficult in practice, these results are in close agreement and suggest that the methodology allows very small fields to be detected and measured.

IV. Discussion

Very weak magnetic field detection is a well-established science, but it often relies on costly or exotic techniques such as superconducting quantum interference device systems [7], which necessitate supercooling and may not be practical for small portable applications. The ability to propagate and detect magnetic fields beyond a steel boundary has many applications, in particular, in the field of nondestructive imaging [8]. For example, it is often required to image and quantitatively assess steel reinforcing bars or cables both embedded in concrete and located below a steel lining [9], [10]. Microwave and radar techniques cannot be deployed in such circumstances since the steel layer represents a totally reflective barrier. By altering the excitation frequency of the magnetic field, it is also possible to induce eddy current flow at different depths in the target bar or cable (due to the skin effect) and, hence, obtain information relating to corrosion severity, cracking, or other surface defects.

The ability of the system to detect the high-frequency magnetic fields is critically dependent on both the resolution of the DSP system and the selectivity of the super narrow-band filter. At 9 kHz, the raw signal voltage produced by the receiver, when directly over the transmitter, is 0.27 μV rms. Since the system can (theoretically) resolve to one part in 1.678×10^7, the minute signals present in the background noise lie above its quantization limits and can therefore be recovered and amplified. The operation of the filter may also be viewed from a different perspective; the convolution integral is given by

$$y(t) = \int_{-\infty}^{\infty} h(\tau)x(t-\tau)d\tau. \tag{10}$$

The integrated energy of the filtered signal therefore increases as the duration of the kernel lengthens; for discrete systems, the increase is proportional to $\sqrt{M}$, where M represents the number of coefficients in the filter. The potential consequence of this relationship is significant; it implies that much higher frequencies than those discussed here could be detected, given appropriate processing algorithms and instrumentation.

It is clear that there is a limitation to this approach, which is ultimately determined by the principle of duality that exists between the frequency and time domains. As the filter bandwidth becomes ever narrower, the ring-down time of its impulse response increases (ultimately, for a filter of an infinitesimal bandwidth, the impulse response is an eternal sinusoid). In this instance, a settling time of 5 s was acceptable, although for higher speed scanning, a stronger initial transmitter field would boost the signal-to-noise ratio, obviating the requirement for such an extreme filter specificity.

The measurement instrumentation described here is not alone in its ability to detect weak magnetic fields; for example, lock-in amplifiers may be employed. The authors have compared the results obtained from this system with those provided by a Bentham 223 lock-in amplifier, which has a quoted sensitivity range of 10 μV to 1 V and a frequency range of 0.5 Hz to 100 kHz. This amplifier was evaluated in place of the DSP system with all other instrumentation remaining in place. It was found that the amplifier was able to detect the signal up to 4.5 kHz but not beyond. The authors appreciate that more sophisticated lock-in amplifiers are available with greater sensitivities, but cost is also a factor that predisposes in favor of the digital approach; the price of a good-quality lock-in amplifier is approximately ten times that of the digital system described here.

There is, moreover, a fundamental reason why the digital filter approach is superior. The system described here can simultaneously interrogate at multiple frequencies; the filter can be designed with several super narrow passbands with no additional overhead with regard to processing or hardware.

In these tests, the use of a large plate enabled the edge effects to be maintained at a safe distance from the receiving coil. It is also important to emphasize that the field strengths generated in these tests were very small. The sensitivity of the receiving coil is directly proportional to its area; by increasing its radius by a factor of ten, the voltage output is increased by two orders of magnitude. The authors are now modifying the system in an attempt to detect signals extending to 20 kHz.

V. Conclusion

We have described new instrumentation that is capable of detecting extremely weak high-frequency magnetic fields. The fields were generated using precise 1- and 9-kHz sine-wave signals applied to a small transmitter coil and detected on the opposite face of a 2-mm-thick ferrous steel plate, which had a very shallow skin depth of approximately 0.137 mm (at 9 kHz). At 9 kHz, the skin effect yields an attenuation of 0.457×10^{-6}. With an estimated field strength on the top surface of the transmitter coil of approximately 0.03 mT, the flux density on the far side of the plate is 1.371×10^{-11} T. To put this in context, the Earth's magnetic field is at least 10 000 times stronger than the fields detected here. The detection of these fields is made possible by the very-high-resolution high-speed DSP system that allows the isolation of the signal from the noise by using super narrow-band filtering, in conjunction with extraordinary levels of pure stable gain—in excess of 10^6. The implications for the possibility of detecting high-frequency magnetic fields propagated through ferrous steel are significant, in relation to communications, surveillance, and nondestructive imaging.

References

[1] D. L. Atherton, "Remote field eddy current inspection," *IEEE Trans. Magn.*, vol. 31, no. 6, pp. 4142–4147, Nov. 1995.

[2] H. Hoshikawa, "Remote field eddy current testing of ferromagnetic double wall tube," *Nondestr. Test. Eval.*, vol. 7, pp. 337–346, 1992.

[3] T. Takagi, "Development of eddy current testing probe for thick-walled metal plate and quantitative evaluation of cracks," *Trans. Jpn. Soc. Mech. Eng.*, vol. 69, pt. A, no. 678, pp. 455–462, Feb. 2003.

[4] T. Naruse, "Investigation of steel thickness measurement by an electromagnetic method using a step exciting current," *Mater. Eval.*, vol. 56, no. 5, pp. 631–635, 1998.

[5] I. J. Won and D. Keiswetter, "Electromagnetic induction spectroscopy," in *Proc. IGARSS*, 1998, vol. 1, pp. 517–519.

[6] P. Gaydecki and B. Fernandes, "An advanced real-time DSP system for linear systems emulation, with special emphasis on network and acoustic response characterization," *Meas. Sci. Technol.*, vol. 14, no. 11, pp. 1944–1954, Nov. 2003.

[7] K. Isawa, S. Takagi, and S. Tosaka, "Tailoring of magnetic imaging system for nondestructive inspection," *J. Magn. Magn. Mater.*, vol. 310, no. 2, pp. e980–e982, Mar. 2007.

[8] F. Yu, C. Zhang, and M. Wu, "On damage evaluation method of the ferromagnetic material based on weak magnetic field detection technology," *Key Eng. Mater.*, vol. 324/325, pp. 331–334, 2006.

[9] B. Fernandes, G. Miller, P. Gaydecki, and M. Zaid, "Preliminary results: A three coil balanced system for imaging steel bars behind steel boundaries," *Nondestr. Test. Eval.*, vol. 21, no. 1, pp. 3–11, Mar. 2006.

[10] G. Miller, H. Hussin, B. Fernandes, M. Zaid, P. Gaydecki, and F. El-Madaani, "A transformer coupling method for imaging defects in concentrically arranged steel tubes," in *Proc. AIP Conf.*, Mar. 2006, vol. 820, no. 1, pp. 713–719.

Patrick Gaydecki (SM'07) received the B.Sc. degree in biology and computer systems from DeMontfort University, Leicester, U.K., in 1980 and the Ph.D. degree in ecological physics from Cranfield University, Cranfield, U.K., in 1984.

He is currently with the Sensing, Imaging, and Signal Processing Group, School of Electrical and Electronic Engineering, The University of Manchester, Manchester, U.K., as a Professor of digital signal processing. His research interests include the design of real-time DSP hardware and software systems for nondestructive testing and biomedical and audio signal applications.

Graham Miller received the B.Sc. degree in electronic engineering and the M.Sc. degree in communication systems engineering from the University of Kent, Canterbury, U.K., in 1997 and 1998, respectively, and the Ph.D. degree in inductive scan imaging from the University of Manchester Institute of Science and Technology, Manchester, U.K., in 2004.

He is currently with the Space Research Centre, University of Leicester, Leicester, U.K.

Muhammad Zaid received the B.Sc. degree in electrical engineering and electronics from the University of Benghazi, Benghazi, Libya, in 1994, the M.Sc. degree in electronics and instrumentation systems from the University of Manchester Institute of Science and Technology, Manchester, U.K., in 2000, and the Ph.D. degree in inductive scan imaging from the University of Manchester in 2005.

He is currently a Senior Lecturer with the School of Applied Sciences, The University of Northampton, Northampton, U.K.

Bosco Fernandes received the B.Sc. degree in mechanical engineering from the University of Glamorgan, Glamorgan, U.K., in 1994 and the M.Sc. degree in instrumentation and analytical science and the Ph.D. degree in inductive scan visualization from the University of Manchester Institute of Science and Technology, Manchester, U.K., in 1995 and 2000, respectively.

He is currently with the School of Electrical and Electronic Engineering, The University of Manchester.

Haitham Hussin received the M.Phil. degree in electromagnetic filed modeling from the University of Manchester, Manchester, U.K., in 2006.

He is currently with the Great Man Made River Authority, Benghazi, Libya.